PHYSICAL REVIEW D **87,** 043509 (2013)

Accounting for baryons in cosmological constraints from cosmic shear

Andrew R. Zentner,[1,2] Elisabetta Semboloni,[3] Scott Dodelson,[4,5,6] Tim Eifler,[7,8]
Elisabeth Krause,[7] and Andrew P. Hearin[1,2,6]

[1]*Department of Physics and Astronomy, University of Pittsburgh, Pittsburgh, Pennsylvania 15260, USA*
[2]*PITTsburgh Particle physics, Astrophysics, and Cosmology Center (PITT PACC), University of Pittsburgh, Pittsburgh, Pennsylvania 15260, USA*
[3]*Leiden Observatory, Leiden University, P.O. Box 9513, 2300 RA, The Netherlands*
[4]*Kavli Institute for Cosmological Physics, Enrico Fermi Institute, University of Chicago, Chicago, Illinois 60637, USA*
[5]*Department of Astronomy & Astrophysics, University of Chicago, Chicago, Illinois 60637, USA*
[6]*Fermilab Center for Particle Astrophysics, Fermi National Accelerator Laboratory, Batavia, Illinois 60510-0500, USA*
[7]*Department of Physics and Astronomy, University of Pennsylvania, Philadelphia, Pennsylvania 19104, USA*
[8]*Center for Cosmology and Astro—Particle Physics, The Ohio State University, 191 W. Woodruff Avenue, Columbus, Ohio 43210, USA*

(Received 31 October 2012; published 5 February 2013)

One of the most pernicious theoretical systematics facing upcoming gravitational lensing surveys is the uncertainty introduced by the effects of baryons on the power spectrum of the convergence field. One method that has been proposed to account for these effects is to allow several additional parameters (that characterize dark matter halos) to vary and to fit lensing data to these halo parameters concurrently with the standard set of cosmological parameters. We test this method. In particular, we use this technique to model convergence power spectrum predictions from a set of cosmological simulations. We estimate biases in dark energy equation-of-state parameters that would be incurred if one were to fit the spectra predicted by the simulations either with no model for baryons or with the proposed method. We show that neglecting baryonic effect leads to biases in dark energy parameters that are several times the statistical errors for a survey like the Dark Energy Survey. The proposed method to correct for baryonic effects renders the residual biases in dark energy equation-of-state parameters smaller than the statistical errors. These results suggest that this mitigation method may be applied to analyze convergence spectra from a survey like the Dark Energy Survey. For significantly larger surveys, such as will be carried out by the Large Synoptic Survey Telescope, the biases introduced by baryonic effects are much more significant. We show that this mitigation technique significantly reduces the biases for such larger surveys, but that a more effective mitigation strategy will need to be developed in order ensure that the residual biases in these surveys fall below the statistical errors.

DOI: 10.1103/PhysRevD.87.043509 PACS numbers: 98.80.−k, 98.35.Gi, 98.62.Py

I. INTRODUCTION

Weak gravitational lensing is a potentially powerful probe of cosmology (e.g., Refs. [1–7]).[1] Imaging surveys such as the Dark Energy Survey (DES) and, in the longer term, the surveys of the Large Synoptic Survey Telescope (LSST), the European Space Agency's Euclid satellite, and the Wide-Field Infrared Survey Telescope expect to measure the power spectrum of cosmological weak lensing with sufficient precision to improve constraints on dark energy dramatically. However, a number of sources of systematic error must be controlled in order to achieve these goals. From a theoretical perspective, it is necessary to predict matter power spectra with precisions of better than one percent over a wide range of scales [9,10]. This is a challenging goal, but significant progress has been realized utilizing N-body simulations containing only dark matter [11–14]. The largest remaining challenge to this goal is to account for the influence of the baryonic component of the Universe in these predictions. Baryonic effects have been shown to alter lensing power spectra significantly on small scales [15–20]. This theoretical systematic error associated with baryonic processes is sufficient to cause large systematic errors in inferred dark energy parameters if unaccounted for Refs. [10,20–22], though Ref. [23] explored methods to cull data in order to protect against scale-dependent uncertainties in predicted power spectra. In the present work, we assess a proposal to mitigate dark energy biases induced by baryonic effects using a method proposed in Ref. [21].

Rudd *et al.* [18] recognized changes in the internal structures of dark matter halos as the cause of the largest alterations to lensing spectra in baryonic simulations (a result confirmed in Refs. [19,20]). Consequently, Zentner *et al.* [21] suggested a strategy to mitigate baryonic effects in forthcoming lensing analyses. Zentner *et al.* [21] proposed altering the canonical relationship between halo mass and halo concentration (e.g., Refs. [24,25]) to account for the matter redistribution precipitated by

[1]This application of lensing goes back more than forty years (e.g., Ref. [8]).

baryonic effects, as this enables the simulations of Ref. [18] to be modeled successfully. Zentner *et al.* [21] then suggested introducing additional parameter freedom into the concentration-mass relation, a necessity because this relation cannot be unambiguously predicted due to the uncertainties in baryonic processes, and fitting the data simultaneously for the parameters that quantify the mass-concentration relation and the cosmological parameters. The value of this strategy is that it can reduce systematic errors (or *biases*) in dark energy parameters to acceptable levels, while increasing the statistical errors on dark energy parameters by only $\sim$10–40%, depending upon the experiment and the complexity of the mass-concentration relation [21] (a similar argument can be made for modified gravity [22]).

Our aim here is to test this mitigation strategy more extensively. We wish to determine if this algorithm will extract cosmological parameters successfully from upcoming survey data. *Successfully* here has a specific and technical meaning, a cartoon version of which is illustrated in Fig. 1. First, success demands that biases in the cosmological parameters due to inaccuracies in theoretical models should be small. There are two biases at play here, the raw bias (the offset of the smaller contour in Fig. 1) before any mitigation is applied and the residual bias (offset of the larger contour in Fig. 1) which remains after fitting for the new free parameters. Ideally, the residual bias will be much smaller than the raw bias; for the method to be truly effective, the residual bias should be smaller than the statistical error. Second, success requires that the additional parameter freedom introduced by the model should not inflate the error bars on cosmological parameters so much as to markedly reduce the constraining power of the experiment. At minimum, the increase in the statistical error bars due to additional parameters should not be so large as to nullify the reduction in the systematic errors.

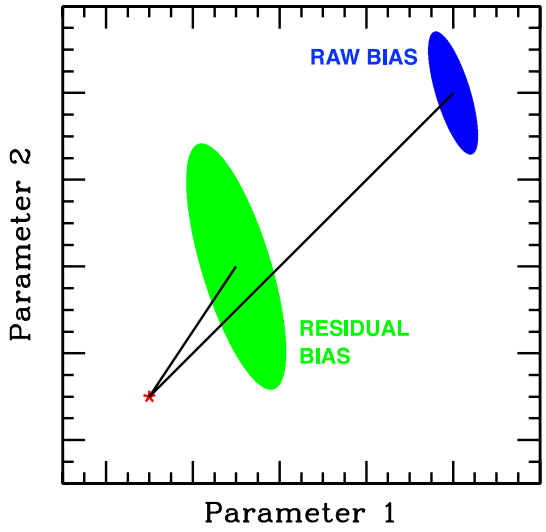

FIG. 1 (color online). Cartoon view of the effect of bias on cosmological parameters (here called "parameter 1" and "parameter 2"). The true value of the parameters is given by the red star. If the bias (in our case, the effect of baryons on the weak lensing power spectrum) is not accounted for, the allowed region in parameter space will be given by the shaded blue region at the top right. The parameters will be offset from their true values, or *biased*. We call the offset in this case the "raw bias." If one attempts to mitigate the bias by introducing new parameters (in our case, allowing for a varying mass-concentration relation), the allowed region will shift to that given by the shaded green contour at the lower left. The errors are now larger due to the increased number of parameters used in the fit, but the offset, which we refer to as the "residual bias," is much smaller than the raw bias.

To carry out this test, we use the results from the OverWhelmingly Large Simulations (OWLS) [20,26,27] as mock data. The OWLS suite consists, in part, of a set of ten simulations, each with the same initial conditions evolved in the context of the same cosmology. One simulation treats only dark matter, while the other nine model baryonic processes using different effective models. We proceed by assuming that each one of the OWLS simulations, in turn, produces the *true* matter power spectrum. We fit each of the OWLS predictions for lensing power spectra with our mitigation model, including nuisance parameters. We compute residual differences in power spectra between our fits and the OWLS predictions and use these differences to estimate the biases in dark energy equation-of-state parameters that would be realized after applying the mitigation scheme. We repeat this analysis in the context of two distinct imaging surveys. The first survey we consider has the precision expected from DES. The second survey we consider represents more long-term, stage IV[2] surveys, such as may be conducted by LSST or Euclid.

We will show that baryonic effects may reasonably lead to raw biases as large as $\sim 2\sigma$–6σ (where σ represents the marginalized statistical error) on dark energy equation-of-state parameters if unaccounted for in the analysis of DES-like data. The size of the bias depends upon the range of multipoles used in the analysis and the baryon model. This broadly confirms prior estimates [20–22]. We will then show that this mitigation scheme can render systematic errors sufficiently small, so as to suggest concentration fitting as an attractive strategy for the cosmological analysis of lensing power spectra from DES. In all cases that we consider, the residual biases remain $\lesssim 0.5\sigma$ and can be kept $\lesssim 0.1\sigma$ if the range of scales included in the cosmological analysis is restricted to $\ell \lesssim 2000$, though restricting scales comes at a non-negligible cost in statistical error.

For stage IV experiments with wide sky coverage, such as LSST or Euclid, the conclusion is slightly more

[2]Using the classification scheme of the Dark Energy Task Force [28], within which DES would be a stage III experiment.

complicated. Absent any mitigation scheme for baryonic process, such future experiments may be subject to raw biases ranging from $\sim 1.5\sigma$ to as large as ten times the statistical error or more. The broad range reflects the differences from one OWLS simulation to the next. However, the largest of these biases are unlikely to be the product of any actual analysis. It seems more likely that the team undertaking the analysis will notice that all models provide poor fits to the data using some "goodness-of-fit" criterion. Nevertheless, it remains imperative to understand the reasons for the poor fits. Our analysis suggests that concentration fitting may reduce systematic errors on dark energy equation-of-state parameters due to baryonic effects to $\lesssim 1.6\sigma$ in the worst case and $\lesssim 0.5\sigma$ in six of the nine simulations we have analyzed. The concomitant increase in the statistical errors is $\lesssim 30\%$. While concentration fitting does alleviate biases in this case, a more sophisticated analysis may be necessary for data of the quality expected from stage IV experiments.

The remainder of this manuscript is organized as follows. In the following section, we describe the lensing power spectra from which we aim to infer cosmological parameters, the details of our modeling procedure, and the cosmological parameters that we consider. We also discuss the Fisher matrix method for estimating statistical and systematic errors in model parameters. In Sec. III, we describe the OWLS simulations and show the differences in lensing power spectra predicted by several of the simulations in the OWLS suite. We describe our simple mitigation model in Sec. IV. Our results for the statistical and systematic errors on dark energy parameters are given in Sec. V, where we address a DES-like experiment, and a future LSST- or Euclid-like experiment in turn. We summarize our results and present our conclusions in Sec. VI.

II. PRELIMINARIES

A. Weak lensing observables

We consider cosmological parameter inference using measurements of cosmic shear from large-scale imaging surveys. We assume that each galaxy has a well-characterized photometric redshift estimate, so that the source galaxies can be binned in N_z photometric redshift bins. We infer cosmological parameters from the $N_{\rm obs} = N_z(N_z+1)/2$ number density-weighted angular convergence power spectra and cross spectra among the galaxies in each of the redshift bins,

$$P_\kappa^{\rm ij}(\ell) = \int {\rm d}z \frac{W_{\rm i}(z) W_{\rm j}(z)}{H(z) D_{\rm A}^2(z)} P_\delta(k = \ell/D_{\rm A}, z). \qquad (1)$$

In Eq. (1), $H(z)$ is the Hubble expansion rate, $D_{\rm A}(z)$ is the angular diameter distance to redshift z, $P_\delta(k, z)$ is the three-dimensional matter power spectrum at wave number k and redshift z, $W_{\rm i}(z)$ are the N_z lensing weight functions, and the lower-case Latin indices indicate the redshift bins (e.g., index i runs from 1 to N_z). The lensing weight functions are

$$W_{\rm i}(z) = \frac{3}{2}\Omega_{\rm M} H_0^2 (1+z) D_{\rm A}(z) \int {\rm d}z' \frac{D_{\rm A}(z, z')}{D_{\rm A}(z')} \frac{{\rm d}n_{\rm i}}{{\rm d}z'}, \qquad (2)$$

where ${\rm d}n_{\rm i}/{\rm d}z$ is the redshift distribution of source galaxies in the ith redshift bin, H_0 is the present Hubble rate, and $D_{\rm A}(z, z')$ designates the angular diameter distance between redshifts z and z'.

The observed spectra $\bar{P}_\kappa^{\rm ij}$, consist of terms due to signal ($P_\kappa^{\rm ij}$) and noise,

$$\bar{P}_\kappa^{\rm ij}(\ell) = P_\kappa^{\rm ij}(\ell) + n_{\rm i} \delta_{\rm ij} \langle \gamma^2 \rangle, \qquad (3)$$

where $n_{\rm i}$ is the surface density of source galaxies in redshift bin i, $\langle \gamma^2 \rangle$ is the intrinsic source galaxy shape noise for each shear component, and $\delta_{\rm ij}$ is the Kronecker delta symbol. The covariance among observables is

$$\mathcal{C}[P_\kappa^{\rm ij}(\ell), P_\kappa^{\rm kl}(\ell)] = \bar{P}_\kappa^{\rm ik} \bar{P}_\kappa^{\rm jl} + \bar{P}_\kappa^{\rm il} \bar{P}_\kappa^{\rm jk}, \qquad (4)$$

assuming Gaussian statistics. Over the range of scales we consider, the Gaussian approximation is reasonable (e.g., Ref. [29]) and greatly simplifies the analysis. Moreover, it is a conservative assumption for our purposes because adopting non-Gaussian covariance generally renders statistical errors larger and diminishes the relative importance of the systematic errors we consider. Throughout this study, we adhere to a common convention by taking $\sqrt{\langle \gamma^2 \rangle} = 0.2$.

B. Survey characteristics and cosmological parameters

We consider cosmological constraints from two representative surveys. The first experiment we consider is based on the specifications of the DES.[3] DES is an example of a near-term, "stage III" project that will exploit cosmic shear measurements to derive constraints on dark energy parameters. We model DES by taking a fractional sky coverage of $f_{\rm sky} = 0.12$, corresponding to approximately 5000 deg^2, and a total surface density of imaged galaxies of $N^{\rm A} = 15$ arcmin^{-2}. This choice is optimistic, but it is a conservative assumption for our purposes, as smaller statistical error bars set a more stringent requirement for the mitigation of systematic errors. We take the DES redshift distribution of source galaxies from the DES Blind Cosmology Challenge simulation. The DES Blind Cosmology Challenge simulation comprises 5000 square degrees of simulated shear maps and is tuned to match the expected observational characteristics of the DES mission.

[3] http://darkenergysurvey.org

We divide the source galaxies into $N_z = 5$ redshift bins such that 20% of the total number of observed galaxies are placed in each bin; this gives $N_{\rm obs} = 15$ distinct convergence spectra. Binning more finely in redshift does not alter our results, in accord with prior studies [10,30]. Throughout the remainder of this paper, we will refer to results based on these survey specifications by the name "DES."

In addition to DES, we will estimate the potential influences of baryonic physics on dark energy constraints from long-term future experiments, categorized as "stage IV" experiments in the report of the Dark Energy Task Force [28]. Examples of potential stage IV experiments that will explore cosmological constraints from weak gravitational lensing are the LSST [31][4] or the European Space Agency's Euclid[5] project [32]. We characterize these experiments by a fractional sky coverage of $f_{\rm sky} = 0.5$ and a number density of source galaxies of $N^{\rm A} = 30\ {\rm arcmin}^{-2}$.[6] Again, these choices are optimistic, but they *maximize* the relative importance of the systematics we aim to militate against, so they are conservative choices for our purposes. We model the redshift distribution of source galaxies in these long-term surveys as $dn/dz \propto z^2 \exp(-(z/z_0)^{1.2})$, with $z_0 \simeq 0.34$ to give a median redshift $z_{\rm median} = 1$. This choice is based on the approximate, observed distribution of high-redshift galaxies [33]. As with DES, we place the source galaxies into $N_z = 5$ redshift bins so that the 20% of the galaxies fall into each bin. We refer to results with these specifications as stage IV results.

We consider cosmologies defined by seven parameters, three of which describe the dark energy. The parameters that describe the dark energy are the contemporary dark energy density in units of the critical density, $\Omega_{\rm DE}$, and the two parameters w_0 and w_a that specify a dark energy equation of state that varies linearly with scale factor, $w(a) = w_0 + w_a(1-a)$ (e.g., Ref. [34]). The parameters of our fiducial cosmology are fixed to match the cosmological parameters assumed in the OWLS simulation program [26]. The parameters specified in the OWLS program are the matter density, $\omega_{\rm M} = 0.1268$, the baryon density, $\omega_{\rm B} = 0.0223$, the scalar spectral index, $n_{\rm s} = 0.951$, the amplitude of curvature fluctuations on a scale of $k = 0.05\ {\rm Mpc}^{-1}$, $\Delta^2_{\mathcal{R}} = 1.9 \times 10^{-9}$ (we actually vary $\ln\Delta^2_{\mathcal{R}}$ about this value), $\Omega_{\rm DE} = 0.762$, $w_0 = -1$, and $w_a = 0$. These parameter values imply that the root-mean-square matter density fluctuation on a scale of $8h^{-1}$ Mpc is $\sigma_8 = 0.74$. We include prior constraints on these parameters that reflect expected limits from the Planck cosmic microwave background anisotropy measurements in all of our calculations. The Planck prior matrix that we use was computed in Ref. [35]. In addition to these seven cosmological parameters, we introduce three other parameters, described in Sec. IV, that account for baryonic effects.

[4]http://www.lsst.org

[5]http://sci.esa.int/euclid

[6]The sky coverage of Euclid will likely be closer to $f_{\rm sky} \approx 1/3$ [32].

C. Methodology

In principle, we propose to assess the effectiveness of the mitigation approach proposed in Ref. [21] using the following steps.

(1) Take the lensing spectra predicted by one of the OWLS simulations as mock data.
(2) Fit the mock data to a model by varying 7 cosmological parameters and determine the statistical errors on the cosmological parameters. This model *does not* include the effects of baryons.
(3) Determine the *raw bias* as the difference between the resulting best-fit dark energy parameters and the "true" input parameters used to generate the OWLS simulations.
(4) Fit the mock data again to a model with those same 7 cosmological parameters as well as 3 additional parameters that account for baryonic effects.
(5) Determine the *residual bias* as the difference between this second fit and the true values of the dark energy parameters used in the OWLS simulations.
(6) Compare the size of the error bars in both cases to see the amount by which the errors are inflated as a result of the new degrees of freedom.
(7) Repeat for each of the OWLS simulations to arrive at nine distinct assessments.

In practice, going through this entire process for all the cases of interest would be extremely time consuming, because fitting for the cosmological and concentration parameters in the multidimensional parameter space that we explore is a computationally expensive task. Instead, we proceed using an approximation, based on both direct fitting for model parameters and Fisher matrix (described below) estimates for the statistical and systematic errors in model parameters. However, it is important to stress that we are assessing the residual bias that will ensue if analysts follow the mitigation strategy proposed in Ref. [21] on upcoming data sets.

In order to limit computational effort, we use the Fisher information matrix to assess the constraining power of these $N_{\rm obs}$ observable spectra. We assume that the spectra are independent, Gaussian random variables at each multipole, so that the Fisher matrix may be written as

$$\mathcal{F}_{\rm AB} = \mathcal{F}^{\rm P}_{\rm AB} + \sum_{\ell=\ell_{\rm min}}^{\ell_{\rm max}} (2\ell+1) \times f_{\rm sky} \sum_{\rm i=1}^{N_z} \sum_{\rm j=i}^{N_z} \sum_{\rm k=1}^{N_z} \sum_{\rm l=k}^{N_z} \frac{\partial P^{\rm ij}_\kappa(\ell)}{\partial p_{\rm A}} \mathcal{C}^{-1}[P^{\rm ij}_\kappa(\ell), P^{\rm kl}_\kappa(\ell)] \frac{\partial P^{\rm kl}_\kappa}{\partial p_{\rm B}}. \quad (5)$$

The matrix $\mathcal{F}^{\rm P}_{\rm AB}$ represents the prior constraints on the cosmological parameters, $p_{\rm A}$ are the parameters of the model, and $\mathcal{C}^{-1}[P^{\rm ij}_\kappa, P^{\rm kl}_\kappa]$ is the inverse of the covariance matrix between observables. The upper-case Latin indices signify model parameters. The parameter $f_{\rm sky}$ specifies the fraction of sky observed in the survey, and the sum runs over multipoles from $\ell_{\rm min}$ to $\ell_{\rm max}$. We take $\ell_{\rm min} = 2f_{\rm sky}^{-1/2}$; however, all of the constraints we consider are dominated by multipoles significantly higher than $\ell_{\rm min}$ so that this choice is inconsequential. We take $\ell_{\rm max} = 5000$ throughout most of our study so as to remain in a regime in which a number of simplifying assumptions are approximately valid (e.g., Refs. [29,36–40]), but we explore other choices of a maximum multipole. Including such high multipoles in our analysis may well be overly optimistic. However, using higher multipoles (smaller scales) in the cosmological analysis results in greater constraining power, so it is interesting to determine the utility of our mitigation scheme out to relatively high multipoles. The Fisher matrix approximates the covariance among model parameters at the maximum of the likelihood, so that the error in the estimate of the Ath parameter can be approximated as $\sigma(p_{\rm A}) = \sqrt{\mathcal{F}^{-1}_{\rm AA}}$, after marginalizing over the remaining parameters.

The Fisher matrix formalism provides a straightforward estimate of parameter biases due to undiagnosed, systematic offsets in observables. Let $\Delta P^{\rm ij}_\kappa$ represent the difference between the true observable and the observable perturbed due to some systematic effect. A Taylor expansion about the maximum likelihood gives an estimate of the systematic error contribution to model parameter $p_{\rm A}$ due to the systematic offsets in observables [41]:

$$b(p_{\rm A}) = \sum_{\rm B} \mathcal{F}^{-1}_{\rm AB} \sum_\ell (2\ell+1) f_{\rm sky} \times \sum_{\rm i,j,k,l} \Delta P^{\rm ij}_\kappa \mathcal{C}^{-1}[P^{\rm ij}_\kappa(\ell), P^{\rm kl}_\kappa(\ell)] \frac{\partial P^{\rm kl}_\kappa}{\partial p_{\rm B}}. \quad (6)$$

The sums over observable (lower-case Latin) indices in Eq. (6) have the same form as those in Eq. (5), though we have written them as a single sum for brevity.

The practical strategy that we implement in an effort to limit computational expense is a modification to the ideal strategy that we would, in principle, pursue as describe above. We *repeal and replace* step 2 through step 5 with the following steps.

(1) Determine the raw bias using the Fisher matrix relation [Eq. (6)] with the systematic offsets in power spectra given by the difference between the OWLS baryonic simulation and the fiducial OWLS simulation that treats dark matter only.
(2) Fit the 3 parameters of the concentration-mass relation of halos to the OWLS convergence power spectra within a *fixed* cosmological model. This results in a best-fit concentration-mass relation that best describes the OWLS simulations within the true underlying OWLS cosmological model.
(3) Compute the residual differences between the predicted convergence spectra from the OWLS simulations and those predicted by the best-fit concentration-mass model with cosmological parameters fixed to the OWLS cosmological model. These residual differences, $\Delta P^{\rm ij}_\kappa$, will give rise to systematic errors in inferred cosmological parameters.
(4) Use the Fisher matrix formalism [particularly Eq. (6)] to estimate the residual bias from $\Delta P^{\rm ij}_\kappa$ after allowing for parametric freedom in the concentration-mass relation. This level of bias will not be removed by fitting for halo structure and will remain in the error budget on cosmological parameters.

This strategy enables us to estimate the efficacy of the baryonic physics mitigation proposal. Additionally, it requires explicitly fitting for only the concentration-mass relation (a 3-dimensional subspace of the full parameter space), so that the computational effort required is significantly less than would be required to fit for halo structure and cosmology simultaneously. The merit of this approach is that the fit allows us to assess the fidelity with which we can model lensing power spectra including baryonic effects, and it brings our fiducial model closer to the true, underlying model prior to applying the Fisher formalism in step 5′. This modified procedure introduces a possible source of confusion. One might think that our final statistical and systematic error estimates do not include the covariance between cosmological and concentration parameters. We emphasize that this is not the case. The Fisher matrix formalism for computing biases in model parameters accounts for the covariance among all the model parameters. The limitation is the standard caveat that the Fisher matrix is a first-order approximation about the maximum likelihood.

III. SPECTRA FROM SIMULATIONS

We estimate the influence of baryonic processes on weak lensing power spectra using the OWLS [20,26,27]. The OWLS suite includes a set of ten simulations set within the same cosmological model that evolve from the same initial conditions to redshift $z = 0$. One of these simulations, the "DMONLY" simulation, treats the gravitational evolution of dissipationless dark matter only. This type of dissipationless dark matter simulation is similar to the vast majority of simulations that have been used to model the observations of contemporary and future surveys. The remaining nine simulations include the baryonic component of the Universe along with various effective models for baryonic gas cooling, star formation, and a number of feedback processes. It is not feasible to simulate these

processes directly, so baryonic simulations rely on a variety of effective models for these processes. Effective models for baryonic processes remain quite uncertain, and it is not possible to produce a definitive prediction for the influences of baryonic processes on observables, such as convergence power spectra. The utility of a simulation suite such as OWLS is that it provides a range of distinct, but plausible, predictions for observables so that systematic errors induced by our ignorance of baryonic physics can be estimated. An important advantage of the test that we present here is that we are applying a mitigation strategy developed on the simulations of Rudd *et al.* [18] to an independent set of simulations that were performed using markedly different simulation strategies. The details of the OWLS simulations have been given in Refs. [26,42–46], while the OWLS power spectra were the subject of Ref. [27], to which we refer the reader as these details are not of immediate importance in the present paper. Follow-up studies by McCarthy *et al.* [47] and McCarthy *et al.* [48] suggest that the properties of galaxies and hot gas in galaxy groups are modeled most reliably in the "AGN" simulation, which includes strong feedback from active galactic nuclei.

We regard each of the nine baryonic simulations separately as a potential realization of the effects of baryons on convergence power spectra. Accordingly, we treat the convergence spectra from *each* of the OWLS baryonic simulations as "observed" spectra that must be modeled faithfully in order to extract reliable constraints. The aim is to test whether a specific strategy to mitigate the influence of baryonic processes on dark energy constraints can be applied to a variety of distinct predictions successfully. *Success* in this context means that the mitigation procedure renders the biases in dark energy parameters significantly smaller than the expected statistical errors. If a *single* mitigation strategy were to achieve the requisite reduction in dark energy parameter biases for *all* plausible simulations, it would be a strong indication that the mitigation strategy may be applied to observational data to limit systematic errors on dark energy parameters associated with the influences of baryons.

van Daalen *et al.* [27] used the OWLS simulations to study the effects of baryonic physics on the matter power spectrum. We use the 3D matter power spectra, $P_\delta(k, z)$, provided in Ref. [27] for the OWLS simulations to estimate convergence power spectra using Eq. (1). In practice, the tabulated matter power spectra from Ref. [27] cannot be used directly to predict convergence power spectra. Due to computational limitations, the OWLS simulation volumes are relatively small (cubic boxes $L = 100h^{-1}$ Mpc on a side) and are subject to significant sample variance and finite volume effects on large scales. In order to overcome these drawbacks, we utilize the OWLS $P_\delta(k, z)$ tables directly for wave numbers $k > 0.314h$ Mpc^{-1}. The OWLS spectra are reliable for $k < 10h$ Mpc^{-1} [27], which is sufficient for our purposes [10]. For wave numbers $k < 0.314$, we use the halo model as implemented in Ref. [21] to estimate the matter power spectrum. We multiply the halo model power spectra by a correction factor that ensures that the two spectra agree at $k = 0.314h$ Mpc^{-1}. In the OWLS simulations, baryonic effects induce changes in power spectra of $\lesssim 1\%$ on scales $k \lesssim 0.314h$ Mpc^{-1}. An important caveat to our approach is that we assume that the effects of baryons on scales $k \lesssim 0.3h$ Mpc^{-1} are insignificant.

Figure 2 shows the fractional differences between the convergence power spectra predicted by the baryonic simulations compared to the DMONLY simulation. For simplicity, we show only the power spectrum in our third DES redshift bin, P_κ^{33} ($0.5025 \leq z < 0.6725$ for our DES model). The predictions for the other fourteen observables show similar features. Figure 2 shows these residuals in several distinct ways. The shaded band is the envelope of

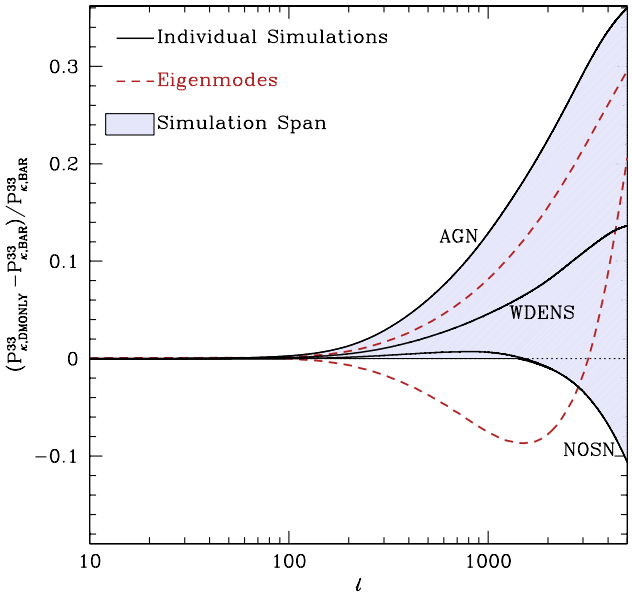

FIG. 2 (color online). Convergence power spectrum residuals between the DMONLY simulation and baryonic simulations (denoted "BAR" in the vertical axis label). For simplicity, this figure shows only the residual for the auto power spectra in the third tomographic bin ($0.5025 \leq z \leq 0.6725$), P_κ^{33}, assuming a DES analysis. Fractional residuals of the other fourteen observables display similar features. The shaded band covers the region spanned by the residuals of all of the OWLS baryonic simulations. The three *thick, solid* lines show three specific simulations that contribute to this band, namely, the AGN (bounding the shaded region above), NOSN (bounding the shaded region below for $\ell \gtrsim 2000$, and WDENS (intermediate) simulations. The residuals at different multipoles are highly correlated. The *dashed* lines show the principal modes of the residuals that have the highest (upper) and second-highest (lower) variance. These modes account for over 90% the variance among the spectra and demonstrate the correlated manner in which baryons alter lensing power spectra.

the power spectrum residual constructed from all nine of the baryonic simulations. The residual power spectra from three specific simulations, namely AGN (bounding the shaded region above), NOSN (bounding the shaded region below for $\ell \gtrsim 2000$), and WDENS (intermediate), are shown as solid lines.

As is evident in the AGN, NOSN, and WDENS models, the deviations in the spectra predicted by the baryonic simulations, differ from the DMONLY simulation in a way that is correlated from multipole to multipole. Accordingly, the shaded bands in Fig. 2 represent the *envelope* of deviations, while an individual spectrum will not range over the shaded area. To represent the typical shapes of the baryonic simulation spectra, we have performed the following exercise. We have computed the covariance among the distinct spectra of the baryonic simulations, $\mathcal{C}[P_\kappa^{33}(\ell), P_\kappa^{33}(\ell')] = N^{-1}\sum_{i=1}^{N}(P_\kappa^{33,\mathrm{i}}(\ell) - \langle P_\kappa^{33}(\ell)\rangle)(P_\kappa^{33,\mathrm{i}}(\ell') - \langle P_\kappa^{33}(\ell')\rangle)$, where i is an index designating the simulation, $N = 9$ is the number of baryonic simulations, and $\langle P_\kappa^{33}(\ell)\rangle$ is the average of the spectra from all of the simulations. We then diagonalized the covariance matrix, $\mathcal{C}[P_\kappa^{33}(\ell), P_\kappa^{33}(\ell')]$. The eigenvectors of the covariance matrix represent the principal modes of variation of the power spectra, and the eigenvalues represent the variance accounted for by the corresponding eigenvectors. The dashed lines in Fig. 2 are the two eigenvectors corresponding to the first- and second-largest eigenvalues. These principal modes account for over 90% of the variance among the spectra and illustrate the correlated manner in which the baryonic simulation spectra may differ from the DMONLY predictions.

IV. FITTING FOR BARYONIC EFFECTS WITH HALO CONCENTRATIONS

Motivated by prior studies indicating that the largest effect of baryons on convergence spectra on relevant scales is a modification of halo structure [18,21], we pursue a mitigation strategy in which baryonic effects are entirely encapsulated into changes in the internal mass distributions within dark matter halos. It is certainly not true that the *only* effect of baryons is to alter halo structures. For example, the distribution of halo masses changes slightly (e.g., Refs. [18,49]), and baryonic effects extend beyond halo virial radii (e.g., Refs. [18,27]). Our goal is to determine the practical utility of such a model in analyses of forthcoming data.

We assume that the average mass distributions within dark matter halos can be described by the Navarro, Frenk, and White density profile [50],

$$\rho(r) \propto \frac{1}{(cr/R_{200\,\mathrm{m}})(1 + cr/R_{200\,\mathrm{m}})^2}. \tag{7}$$

The parameter c is the halo concentration, and the density profile is normalized by our definition of a halo as a spherical object within which the mean density is 200 times the mean density of the Universe, $\rho_{\mathrm{vir}} = 200\rho_{\mathrm{M}}$. Therefore, halo mass and radius are related by $m = 4\pi\rho_{\mathrm{vir}}R_{200\,\mathrm{m}}^3/3$, so that the profile can be normalized by $m = 4\pi\int_0^{R_{200\mathrm{m}}}\rho(r)r^2\mathrm{d}r$ for a given mass and concentration. Halo concentrations predicted by dissipationless simulations of dark matter only have been studied extensively (recent examples are Refs. [24,25,51–53]). The relationship between halo concentration, halo mass, and redshift in the OWLS DMONLY simulation can be adequately characterized by a power-law distribution [27,54,55],[7]

$$c(M, z) = c_0\left(\frac{M}{M_p}\right)^{-\alpha}(1 + z)^{-\beta}, \tag{8}$$

with $c_0 = 7.5$, $\alpha = 0.08$, and $\beta = 1$, in broad agreement with prior studies. The parameter M_p is a pivot mass, which we take to be $M_p = 8 \times 10^{13}h^{-1}\ \mathrm{M}_\odot$. We choose the pivot mass to be close to the halo mass that is most well constrained by lensing spectra [21].

We describe modifications to halo structure through a modified concentration relation, following Refs. [18,21]. In particular, we allow the parameters c_0, α, and β in Eq. (8) to vary in order to describe convergence power spectra within the baryonic OWLS simulations. We determine the values that best capture the simulation results as follows. For each simulation, we produce a set of N_z convergence power spectra. We fit the spectra by minimizing

$$\chi^2 = \sum_{\ell=\ell_{\mathrm{min}}}^{\ell_{\mathrm{max}}}(2\ell + 1)f_{\mathrm{sky}}\sum_{\mathrm{i,j,k,l}}\delta P_\kappa^{\mathrm{ij}}(\ell) \times \mathcal{C}^{-1}[P_\kappa^{\mathrm{ij}}(\ell), P_\kappa^{\mathrm{kl}}(\ell)]\delta P_\kappa^{\mathrm{kl}}(\ell), \tag{9}$$

where $\delta P_\kappa^{\mathrm{ij}}(\ell)$ is the difference between the model and the simulation prediction, for the concentration parameters c_0, α, and β at fixed cosmology. This results in best-fit values for the concentration parameters and residual differences between the best-fit modified concentration models and the predicted spectra from the baryonic simulations. In this manner, we assess the ability of the modified concentration model to describe the baryonic simulations.

The implementation of our model for the effect of modified concentrations on convergence power spectra is based upon the halo model for $P_\delta(k, z)$. The details of the

[7]The fit values come from Ref. [54] after applying a correction to change the pivot mass to M_p at $z = 0$. Reference [54] explored a set of simulations that differ slightly from the OWLS simulations that we examine here. References [27,55] confirm that the OWLS DMONLY simulation has a very similar concentration-mass relation but do not provide detailed fits to the concentration-mass relation as a function of redshift. For the purposes of the present paper, this relation serves only to establish a baseline with respect to which we model the remaining baryonic simulations. Plausible alterations to the baseline model, given the results quoted in Refs. [54,55], cause only minor quantitative changes to our subsequent results.

halo model implementation are described in Ref. [21]. However, using the halo model to fit convergence power spectra from the OWLS simulations introduces a nontrivial complication. On large scales, the halo model predictions for $P_\delta(k, z)$ are systematically offset from the OWLS simulation predictions because of the finite volumes of the simulations. To overcome this, we proceed as follows. For each trial value of the halo concentration parameters, we compute a matter power spectrum offset $\Delta P_{\delta,\mathrm{HM}}(k, z)$ between the fiducial halo model with the standard values of c_0, α, and β and the halo model prediction with our trial values of the concentration parameters. We then compute our trial matter power spectrum, which we use to predict convergence and compute χ^2, by adding the offset defined by the halo model to the DMONLY prediction, $P_{\delta,\mathrm{trial}}(k, z) = P_{\delta,\mathrm{DMONLY}}(k, z) + \Delta P_{\delta,\mathrm{HM}}(k, z)$. In other words, we utilize the halo model to estimate a correction to be applied to the DMONLY matter power spectra. In this manner, the spectra are not offset systematically with respect to each other on large scales. This strategy mimics what would likely have to be done in any analysis of real data; the predictions of dissipationless dark matter simulations would be established, but a correction would need to be applied to account for baryonic effects. This is the same strategy suggested in Ref. [18] and adopted by Ref. [20].

Figure 3 summarizes the results we obtained by fitting concentrations to describe the baryonic OWLS simulations. The figure shows the difference between the power spectra in the best-fit models with modified concentrations and the true baryonic simulations. This is analogous to Fig. 2. As in Figs. 2 and 3, shows only residuals of the autocorrelation for sources in the third DES photometric redshift bin, in the interest of clarity. The most obvious feature of Fig. 3 is that the fit residuals are nearly an order of magnitude smaller than the differences between the baryonic and DMONLY simulations. The correlated structure of the fit residuals is also shown in Fig. 3 by the two principal modes that account for the majority of the variance in the spectra among the baryonic OWLS simulations. The two modes depicted in Fig. 3 account for nearly 97% of the variance among the spectra in the third redshift bin.

The residuals in Fig. 3 represent the remaining systematic errors in the predictions of convergence power spectra after accounting for baryonic effects using a simple, phenomenological model. These systematic offsets will propagate into biases in the estimators of the cosmological parameters. We explore this in detail in the next section.

The best-fit concentrations are given in Table I. The concentrations of the dark matter halos in the OWLS simulations have been presented in Duffy *et al.* [55]. The concentrations we quote in Table I exhibit two important deviations from the results quoted in Ref. [55]. First, our fit to the AGN simulation results in significantly lower concentrations. This could be because mass that would be within the DMONLY virial radii of these halos is moved outside of the virial radii in the AGN simulation, and the concentrations are driven to low values to account for this effect. The OWLS collaboration has argued that the AGN simulation is the most realistic among their suite, so a genuine discrepancy in this case could have important implications for our method. Second, our fits generally yield a stronger mass dependence than the OWLS fits.

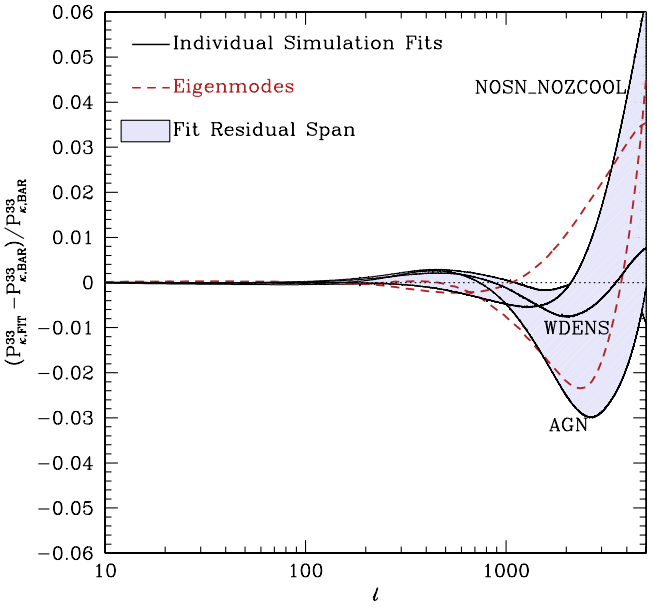

FIG. 3 (color online). Convergence power spectrum residuals between our halo model fits to the spectra predicted by the baryonic simulations and the baryonic simulation predictions themselves. The shaded band shows the envelope containing the fit residuals for all of the OWLS baryonic simulations, analogous to the shaded band in Fig. 2. As in Fig. 2, the thick, solid lines show examples of the fit residuals from specific cases, namely the AGN (lowest at high multipole), NOSN_NOZCOOL (highest at high multipole, lowest at $\ell \lesssim 1000$), and WDENS (intermediate) simulations. It is evident that the envelope containing all residuals is comprised by different simulations over different multipole ranges. The dashed lines show the two principle modes of the residuals with the highest variance. These represent correlated failure modes of the fitting procedure. This figure is to be compared to Fig. 2, but notice that the ranges on the ordinal axes are considerably different in the two figures. The halo model fits typically reduce power spectrum residuals by more than an order of magnitude.

A comparison of between our concentration results is not trivial for several reasons. Foremost among these, Ref. [55] quotes the effective concentrations of dark matter, while lensing is sensitive to all matter. The concentrations that we quote are the effective concentrations of all matter (baryonic as well as dark). Reference [55] does provide nonparametric measures of total matter concentration; however, these measures exhibit behavior different from the Navarro, Frenk, and White profile fits, and it is unclear how they correspond to the result of our

TABLE I. Concentration parameters that best fit the OWLS simulation spectra. The best-fit values are given for the normalization of the concentration relation c_0, in units of the normalization for the DMONLY simulation, the power-law index specifying the mass dependence α, and the power-law index of the redshift dependence, β. The values in this table correspond to the specific case of DES with $\ell_{\rm max} = 5000$. The other cases we explore yield very similar best-fit concentrations. The errors on the best-fit parameters are set by the survey characteristics and are not appropriate for direct comparison to the published OWLS results.

Simulation	$c_0/c_0^{\rm DMONLY}$	α	β
REF	1.13	0.20	0.83
WML4	1.14	0.18	0.91
NOSN	1.20	0.27	0.50
NOZCOOL	1.16	0.16	0.91
WDENS	0.96	0.20	1.39
WML1V848	1.09	0.22	1.33
DBLIMFV1618	0.89	0.24	1.23
NOSN_NOZCOOL	1.41	0.40	1.44
AGN	0.34	0.79	2.06

fitting procedure. Additionally, the lensing signal on the scales that we explore is sensitive to mass redistribution on scales near halo virial radii and insensitive to halo profiles on significantly smaller scales. Therefore, it is not clear that our exercise should yield the same concentrations as those derived from fitting profiles directly because the two procedures are not equally sensitive to halo structure at all scales. Furthermore, we have assumed power-law relationships between halo concentration, halo mass, and redshift. This can be justified by the fact that lensing is sensitive to a relatively narrow range of halo masses and redshifts [21], so that the power-law indices that we recover may not correspond to those derived from a fit to simulation results over a wide range of masses and redshifts. As a results of these complicating factors, we reserve a more detailed comparison between our concentration parameters and those of the simulations for future work.

V. COSMOLOGICAL CONSTRAINTS AND RESIDUAL BIAS

In this section, we project the effects of baryons in simulations onto cosmological parameters. We begin by discussing our results in the context of the DES and conclude the section with a brief discussion of possible cosmological biases for stage IV experiments such as LSST or Euclid.

It is useful to consider the baseline constraints on the dark energy equation-of-state parameters. We consider two cases that will prove useful in the following. The first case corresponds to standard constraint projections on the dark energy equation-of-state parameters assuming that the nonlinear growth of structure is known perfectly. In the context of our analysis, this means that the concentrations of halos are known perfectly, and we refer to these constraints as "fixed-C" constraints accordingly. As we are exploring a mitigation strategy in which we fit for concentrations concurrently with cosmological parameters, it is necessary to assess the degradation in dark energy parameter constraints due to this additional freedom. We refer to constraints derived from an analysis in which concentrations are fit alongside cosmological parameters as "fit C".

A. Results for the Dark Energy Survey

Our baseline constraints for DES, as well as the degradation in constraints when concentrations are fit alongside cosmological parameters, are shown as a function of the maximum multipole used in the analysis in Fig. 4. Figure 4 contains four panels. The two panels on the left show results for w_0, while the two panels on the right show results for w_a. The top panels show the marginalized constraints on the equation-of-state parameters as a function of the maximum multipole used in the analysis. The solid lines show the marginalized constraints in the standard fixed-C case, while the dashed lines show constraints in the fit-C case, in which concentrations are permitted to vary. The lower panels show the ratio of the fit-C constraints to the fixed-C constraints at each multipole, giving the factor by which introduction of the additional nuisance parameters describing concentrations degrades the constraints.

It is clear that constraints are degraded if the concentration-mass relation of dark matter halos must be allowed to vary. This degradation is mild ($\lesssim 20\%$) if the maximum multipole used in the cosmological analysis is $\ell_{\rm max} \lesssim 3000$ and increases to $\gtrsim 40\%$ once scales to $\ell_{\rm max} \approx 5000$ are included. The level of degradation depicted in Fig. 4 is slightly larger than that estimated in Ref. [21] for a DES-like experiment. We find that this discrepancy is almost entirely due to the fact that the source redshift distribution used in the present study differs significantly from that assumed in Ref. [21]. In particular, the redshift distribution that we assume concentrates source galaxies at significantly lower redshift, resulting in relatively lower lensing power compared to noise and reducing the lever arm to high redshift sources.

To determine the impact of this mitigation scheme on the dark energy program of a particular experiment, such as DES, the degradation in cosmological parameters caused by fitting for the concentrations of halos must be compared to the biases in these parameters that may be realized if baryonic effects are neglected. We compute these biases by using the residuals between the DMONLY and baryonic simulations as the systematic offsets in Eq. (6). An example of these offsets is depicted in Fig. 2.

The maximal biases that are induced by neglecting baryonic effects in our analysis of the OWLS simulations are shown as the outer (blue) bands in Fig. 5 (for w_0) and

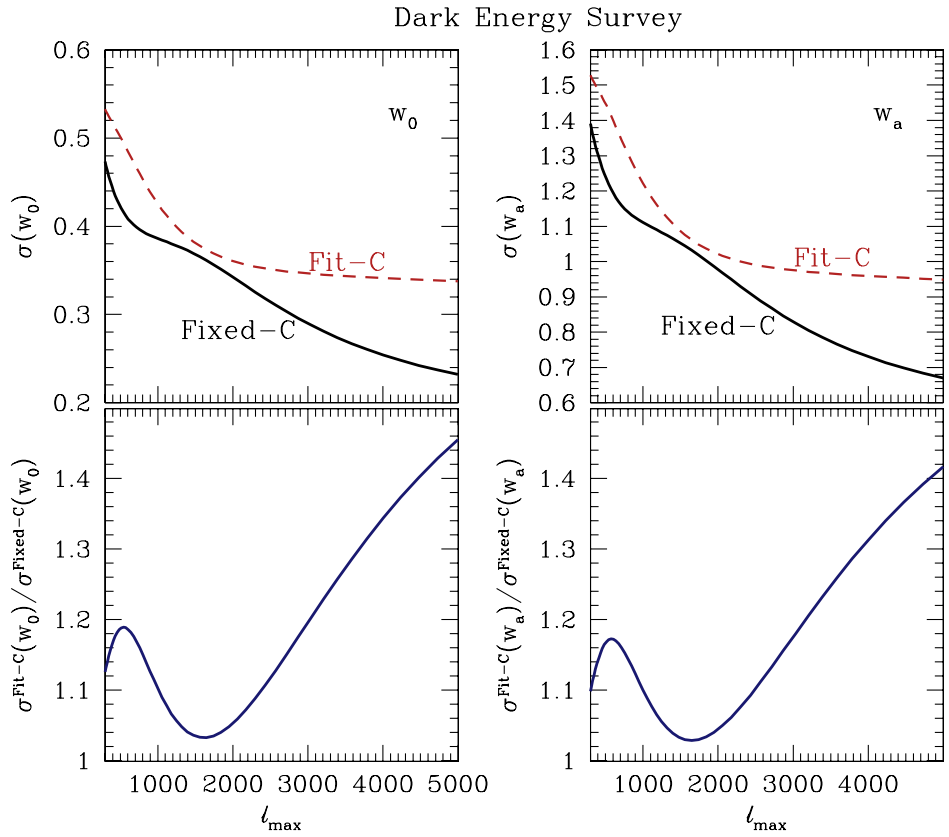

FIG. 4 (color online). Constraints as a function of maximum multipole used to infer cosmological parameters. The *left* panels show results for w_0, while the *right* panels show results for w_a. In the *top* panels, the solid lines show standard constraints assuming that the power spectrum is known perfectly. The dashed lines show the constraints that may be realized if the halo concentration-mass relation must be fit simultaneously with cosmological parameters. The *bottom* panels show the ratio of the constraints realized when concentrations must be fit, $\sigma^{\text{Fit-C}}$, to the constraints realized in the standard scenario, $\sigma^{\text{Fixed-C}}$. Constraints are significantly degraded beyond $\ell_{\text{max}} \sim 3000$ when the concentration-mass relation is permitted to vary. Constraints on w_0 and w_a show the same qualitative features.

Fig. 6 (for w_a). In particular, the *outer* (*blue*) bands delineate the extremal biases (maximum and minimum as the biases may be positive or negative) induced by analyzing any of the OWLS simulations without accounting for baryonic effects. The outer bands in Fig. 5 and 6 represent the envelope of the bias from all simulations, while for any individual simulation, the bias is a smooth function of maximum multipole. The features in the bands in Figs. 5 and 6 arise when the particular simulation that gives rise to the extremal bias changes from one multipole to the next.

The biases induced by neglecting baryonic effects in Figs. 5 and 6 are as large as $\sim 3\sigma$ for w_0 and w_a if the analysis includes multipoles out to $\ell_{\text{max}} \approx 3000$. Including multipoles out to $\ell_{\text{max}} \approx 5000$ drives the maximal potential bias to $\sim 6\sigma$. These bias levels have a clear significance for the effort to understand dark energy. However, we remind the reader that we have used the Fisher matrix approximation to estimate the biases on cosmological parameters. A necessary caveat to our results is that Eq. (6) is the lowest-order approximation to the bias in the limit of small parameter biases and may not provide an accurate bias estimate for large biases. Nevertheless, the statement that the biases are significant ($\gtrsim 1\sigma$) in this case is robust.

The inner (orange) bands in Figs. 5 and 6 delineate the extremal range of dark energy equation-of-state parameter biases realized after fitting for the halo concentration-mass relation in the baryonic simulations and using the fit to correct the power spectra as described in Sec. IV. Specifically, we compute these biases by utilizing the residuals between the *corrected* DMONLY spectra and the baryonic simulations, an example of which is shown in Fig. 3, in Eq. (6). To make Figs. 5 and 6 show fair comparisons of the biases, the biases for the fit-corrected cases are shown in units of the statistical error in the case of fixed C. Showing these biases in units of the statistical error in the case of fit C would reduce their magnitudes in Figs. 5 and 6.

Fitting for concentrations clearly leads to dramatic reductions in parameter biases. Indeed, the biases are typically less than $\sim 10\%$ of the statistical error at low multipoles and never exceed $\sim 50\%$ ($\sim 60\%$) of the

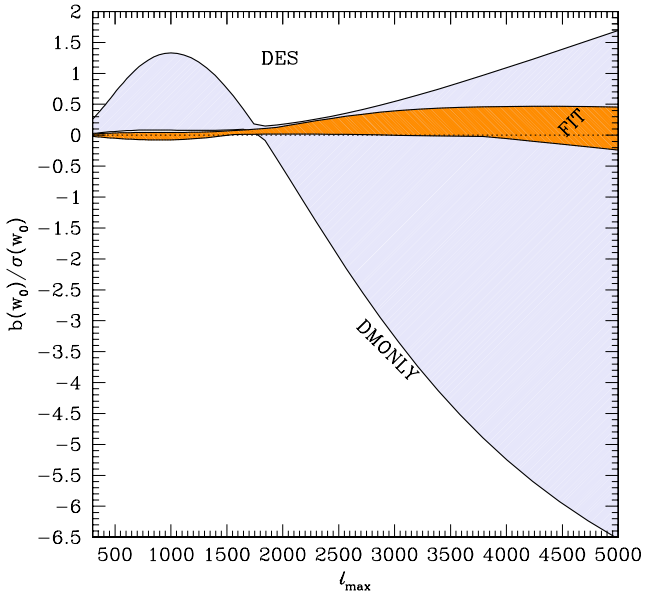

FIG. 5 (color online). Biases induced in the dark energy equation of state parameter w_0 as a function of the maximum multipole used to infer cosmological parameters. The bias is shown in units of the statistical error on w_0 in order to make the relative importance of the systematic error induced by baryons explicit. The outer shaded (blue) band covers the range of biases spanned by computing the biases induced by analyzing all of the OWLS baryonic simulations without any model for baryonic effects. The inner shaded (orange) band shows the range of biases induced by after taking the best-fit concentration model to describe baryonic effects in the OWLS simulations.

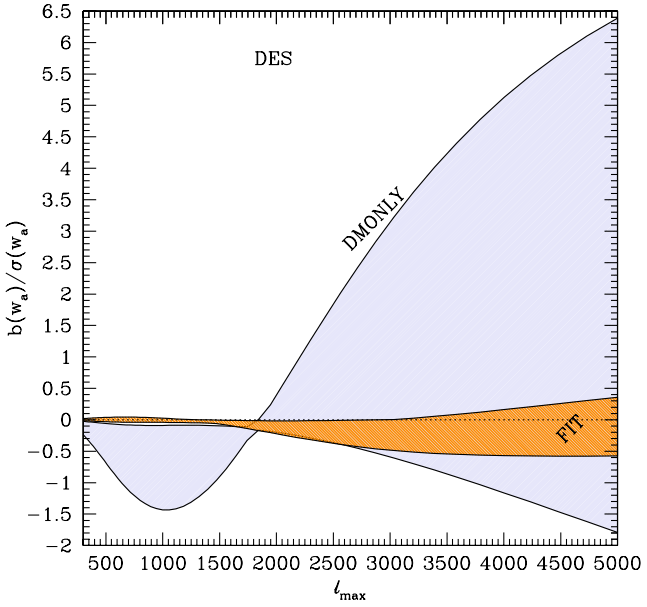

FIG. 6 (color online). Biases induced in the dark energy equation-of-state parameter w_a as a function of the maximum multipole used to infer cosmological parameters. The bias is shown in units of the statistical error on w_a in order to make the relative importance of the systematic error induced by baryons explicit. The outer shaded (blue) band covers the range of biases spanned by computing the biases induced by analyzing all of the OWLS baryonic simulations without any model for baryonic effects. The inner shaded (orange) band shows the range of biases induced by after taking the best-fit concentration model to describe baryonic effects in the OWLS simulations.

statistical error in w_0 (w_a) for $\ell_{\rm max} \lesssim 5000$. This suggests that the mitigation strategy of fitting for a halo concentration relation alongside cosmological parameters will result in a dark energy error budget that is preferable to neglecting baryonic effects. At $\ell_{\rm max} \sim 3000$, fitting for concentration increases the statistical error in w_0, for example, by $\sim$20% compared to the ideal case (Fig. 4), and reduces the systematic error to $\sim$40% of the statistical error (maximum). Taking a simple and conservative approach of adding these two contributions, the resulting error on w_0 increases to $\sim$160% of the constraint in the ideal case. This is to be compared to a potential systematic error in the case where no mitigation for baryonic processes is undertaken of as much as $\sim$350% of the statistical error.

B. Stage IV experiments

Having discussed the utility of the proposed mitigation scheme of Zentner *et al.* [21] for DES, we briefly describe analogous results for forthcoming, stage IV dark energy experiments such as LSST and Euclid. Figure 7 shows cosmological constraints for a stage IV dark energy experiment, including the degradation in those constraints incurred by fitting for the concentrations of halos concurrently with the cosmological parameters. Figure 7 exhibits two notable features compared to the analogous results for DES (Fig. 4). First, the constraints from stage IV experiments are significantly more restrictive, though this is an expected result (e.g., Ref. [28]). Second, stage IV experiments suffer from slightly greater degradation in dark energy parameter constraints when fitting for halo structure along with cosmological parameters. In particular, the degradation in dark energy parameters reaches $\approx 30\%$ at a maximum multipole of $\ell_{\rm max} \approx 3000$ and $\approx 55\%$ at $\ell_{\rm max} \approx 5000$.

The biases resulting from the analysis of stage IV experiments are shown in Fig. 8 (w_0) and Fig. 9 (w_a). Notice that we present the results in a slightly different way for stage IV experiments. In particular, four of the OWLS simulations (“AGN”, “DBLIMFV1618”, “WDENS”, and “WML1V848”) give significantly larger biases than any of the other five simulations. Therefore, we show the biases for these individually in the main panels of Figs. 8 and 9. We show results for the remaining five simulations in the inset panels. In all cases, the value of fitting concentrations to mitigate for baryonic effects in cosmological parameter analyses is apparent. However, notice that the residual biases in the worst cases can remain significant compared to the ideal statistical error even after fitting for the concentration-mass relation. This indicates that a more accurate mitigation scheme will be needed in order to

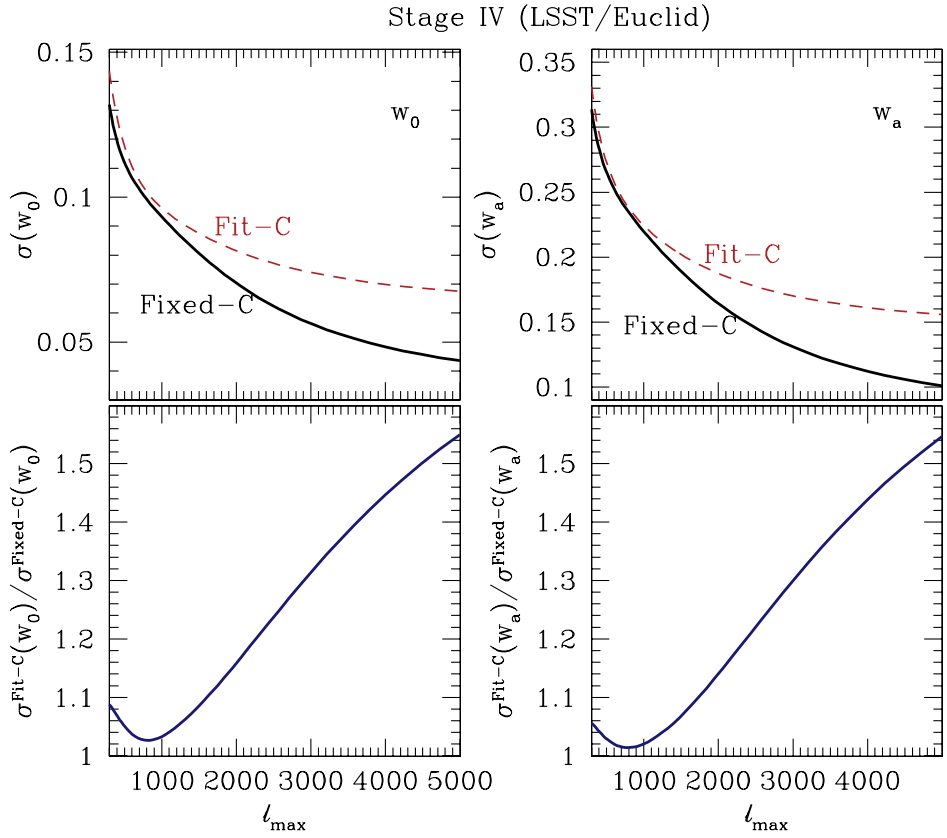

FIG. 7 (color online). Constraints as a function of maximum multipole used to infer cosmological parameters. The panels and lines are as in Fig. 4, but pertain to a stage IV dark energy experiment such as the Large Synoptic Survey Telescope or the European Space Agency's Euclid.

reduce the theoretical systematic associated with baryonic physics to the level of the statistical errors expected of stage IV dark energy experiments.

VI. CONCLUSIONS

We have explored the viability of a strategy to mitigate the influence of baryonic effects on dark energy constraints from cosmological weak lensing. The strategy entails fitting lensing data for both cosmological parameters and the concentration-mass relation of all matter in halos simultaneously. We assessed this scheme by using it to analyze power spectra predicted by a suite of cosmological simulations as though they were genuine data. Specifically, we computed the resultant systematic and statistical errors on dark energy parameters that would be incurred by fitting such data according to this strategy.

We find that introducing additional parameter freedom to describe the concentration-mass relations of halos reduces the systematic errors on dark energy parameters to marginally acceptable levels in all cases. For a DES-like analysis exploiting all multipoles $\ell \leq 3000(5000)$, fitting for concentrations increases statistical errors by $\lesssim 25\%(45\%)$ (Fig. 4) but reduces the potential systematic error by a factor of as much as ~ 7, to $\lesssim 0.3\sigma(0.5\sigma)$, in the worst case scenario (Figs. 5 and 6). The reduction in systematic error outweighs the increase in statistical error suggesting that this mitigation scheme may be a viable option for analyzing data of the quality expected from DES.

For stage IV experiments, such as the surveys to be undertaken by the LSST or Euclid, the conclusion is somewhat less straightforward. What is clear is that some mitigation strategy for baryonic effects is necessary. Systematic errors on w_0 and w_a incurred by fitting the OWLS simulations with no model for baryonic processes can be as large as several tens of the statistical error if all scales $\ell \lesssim 5000$ are included in the analysis (Figs. 8 and 9). Of course, as we mentioned in the introductory section, such large biases are not likely to be realized as the result of any analysis. Rather, it is likely that the analysis team will not find acceptable fits to the observables according to a specific fit criterion. Nevertheless, it is apparent that a model for possible baryonic effects will be necessary in order to extract cosmological parameters reliably.

For stage IV experiments, the strategy of fitting the concentrations of halos in order to militate against large biases in the inferred cosmological parameters, particularly the dark energy equation-of-state parameters, is relatively less effective. One complicating factor is that the different OWLS simulations lead to more disparate

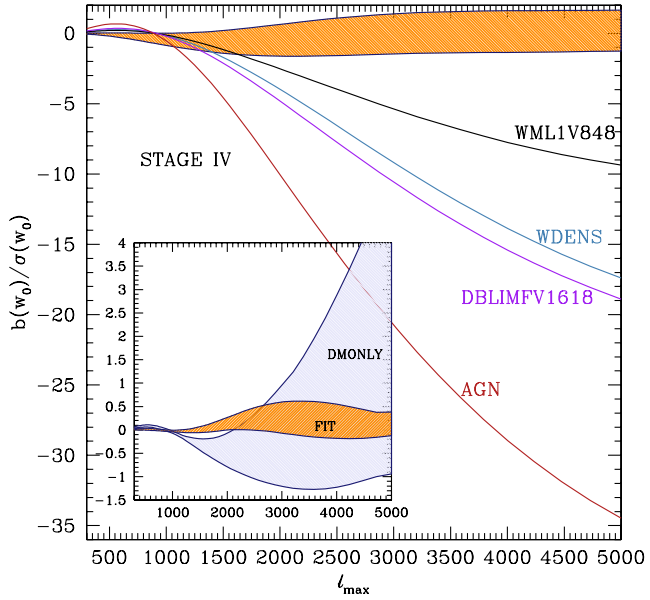

FIG. 8 (color online). Biases induced in the dark energy equation-of-state parameter w_0 from the analysis of a stage IV dark energy experiment as a function of the maximum multipole used to infer cosmological parameters. For stage IV experiments, four of the OWLS simulations lead to biases significantly larger than the others, and it is useful to emphasize this. In the main panel, the biases that result from analyzing those four simulations without any model to account for baryonic effects. These biases are clearly very large. Each line is labeled by the name of the corresponding OWLS simulation in the panel. The shaded (orange) band shows the range of biases that result after taking the best-fit concentration model to describe baryonic effects to analyze these same four simulations. The biases here are significantly reduced but remain non-negligible ($\sim 1\sigma$). The inset panel shows results for the remaining five OWLS simulations. In this case, the inner (orange) and outer (blue) shaded bands are the same as in Fig. 5 for DES. In each of these cases, the mitigation procedure renders biases in the dark energy equation of state parameter w_0 smaller than the statistical error.

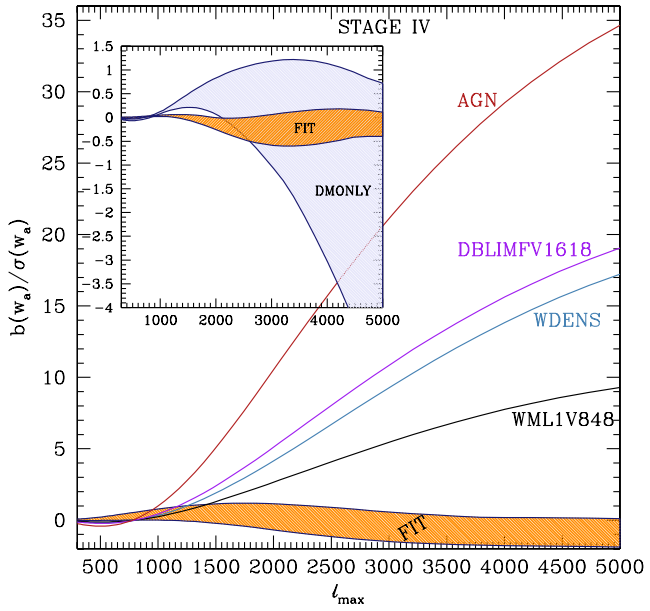

FIG. 9 (color online). Same as Fig. 8, but for the bias on w_a from a stage IV experiment. Notice that the vertical axis is asymmetric about zero.

conclusions in this case. In the worst case, that of the OWLS AGN simulation, the residual biases after fitting for concentrations are $\sim 1.6\sigma$, assuming all scales to $\ell_{\rm max} = 5000$ are included. It is necessary to restrict consideration to multipoles $\ell_{\rm max} \lesssim 1100$ in order to reduce this bias to $\sim 1\sigma$. However, for six of the nine OWLS simulations that we have analyzed, the residual bias including all scales to $\ell_{\rm max} = 5000$ is $\lesssim 0.5\sigma$. The concomitant cost of the additional parameters for the *statistical* errors is $\lesssim 55\%$. Fitting for an effective halo concentration-mass relation does reduce biases in the dark energy equation-of-state parameters; however, in the most extreme cases that we have analyzed, these biases remain significant compared to the statistical errors expected from stage IV experiments.

As pointed out by Zentner *et al.* [21], fitting for an effective concentration-mass relation also yields information that may help to constrain galaxy formation models. In this case, the procedure gives constraints on the parameters of the concentration-mass relation at no additional cost. In the case of DES (stage IV), the best-constrained halos have masses $M \sim 8 \times 10^{13} h^{-1}\ {\rm M}_\odot$ ($M \sim 6 \times 10^{13} h^{-1}\ {\rm M}_\odot$) at redshift $z \sim 0.23$ ($z \sim 0.31$), and constraints on the average concentrations of such halos are $\sigma_c/c \sim 0.06$ ($\sigma_c/c \sim 0.03$). Such constraints may prove useful in understanding the formation histories of galaxies and galaxy clusters.

A handful of other recent studies have investigated methods for marginalizing over uncertainty in power spectra in deriving cosmological constraints from weak lensing [10,20,56,57]. References [10,56,57] explore significantly more general parameterizations. However, they all reach conclusions that are broadly consistent with ours in that each finds self-calibration of uncertainty in the nonlinear matter power spectrum a promising approach. This broad agreement among different approaches likely stems from the well-known fact that cosmological information can be extracted from lensing data based only upon geometrical considerations [58,59]. Reference [20] is most similar to ours. These authors explore a halo-model-based mitigation scheme in which gas and stars are modeled separately from dark matter, similar to the model proposed by Rudd *et al.* [18]. Semboloni *et al.* [20] find that their simple model can significantly reduce dark energy parameter biases for near term surveys, but that improvement may be necessary in order to address stage IV dark energy experiments, a result in broad agreement with ours. However, Semboloni *et al.* [20] did not use their methods to model an *independent* set of simulations, nor did they address the statistical cost of marginalizing over additional parameters in their model.

In summation, our results suggest concentration fitting as a useful and viable strategy with which to analyze cosmological weak lensing power spectra from DES in order to extract constraints on the dark energy equation of state. Based on our analyses, stage IV experiments may remain vulnerable to significant biases in the inferred values of the dark energy parameters even after militating against baryonic effects with concentration fitting. At minimum, estimates for systematic errors such as those presented here should be a component of the error budgets of such experiments.

Future work may be able to improve this situation. For one, simulations such as the OWLS simulations make predictions for the properties of galaxies. It may be possible to compare the properties of galaxies in order to determine which simulations are more likely to represent the observed Universe and use this information to place priors on additional parameters in mitigation schemes (the concentration parameters in our case; see Ref. [21]). The OWLS collaboration has shown that the AGN simulation describes the observed properties of galaxies most successfully [27,47], while our analysis of the AGN simulation for stage IV experiments leaves a non-negligible residual bias. An important and necessary aspect of future efforts to address these issues with simulations will be to develop lensing predictions from baryonic simulations in larger computational volumes. On another front, it may be possible to develop more sophisticated models for the influence of baryons on lensing power spectra that can minimize biases in inferred cosmological parameters without a significant cost in statistical errors. As the cosmological community learns from stage III experiments such as DES and prepares for the stage IV experiments of the coming decade, such efforts should be a high priority in order to maximize the scientific yields of the next generation of dark energy experiments.

ACKNOWLEDGMENTS

This work grew out of a working group meeting hosted by the Aspen Center for Physics. As such, this material is based upon work supported in part by the National Science Foundation under Grant No. PHY-1066293 and the hospitality of the Aspen Center for Physics. We are grateful to Marcel van Daalen, Joop Schaye, and the other members of the OWLS collaboration for making their simulation power spectra available. We thank Henk Hoekstra, Dragan Huterer, Jeffrey Newman, Bob Sakamano, Joop Schaye, and Risa Wechsler for helpful discussions and comments on early drafts of this manuscript. A. R. Z. and A. P. H. were funded by the Pittsburgh Particle Physics, Astrophysics, and Cosmology Center (PITT PACC) at the University of Pittsburgh and by the National Science Foundation through Grant No. AST 0806367. A. P. H. is also supported by the U.S. Department of Energy under Contract No. DE-AC02-07CH11359. E. S. acknowledges support from the Netherlands Organisation for Scientific Research (NWO) Grant No. 639.042.814 and from the European Research Council under the EC FP7 Grant No. 279396. E. S. also acknowledges support from the Leids Kerkhoven-Bosscha foundation. S. D. was supported by the U. S. Department of Energy, including Grant No. DEFG02-95ER40896, and by the National Science Foundation under Grant No. AST-090872. The research of T. E. and E. K. was funded in part by NSF Grant No. AST 0908027 and U. S. Department of Energy Grant No. DE-FG02-95ER40893.

[1] A. Albrecht *et al.*, arXiv:astro-ph/0609591.
[2] H. Hoekstra and B. Jain, Annu. Rev. Nucl. Part. Sci. **58**, 99 (2008).
[3] D. H. Weinberg, M. J. Mortonson, D. J. Eisenstein, C. Hirata, A. G. Riess, and E. Rozo, arXiv:1201.2434.
[4] W. Hu, Astrophys. J. Lett. **522**, L21 (1999).
[5] W. Hu and M. Tegmark, Astrophys. J. Lett. **514**, L65 (1999).
[6] A. Refregier, R. Massey, J. Rhodes, R. Ellis, J. Albert, D. Bacon, G. Bernstein, T. McKay, and S. Perlmutter, Astron. J. **127**, 3102 (2004).
[7] W. Hu and B. Jain, Phys. Rev. D **70**, 043009 (2004).
[8] J. Kristian, Astrophys. J. **147**, 864 (1967).
[9] D. Huterer and M. Takada, Astropart. Phys. **23**, 369 (2005).
[10] A. P. Hearin, A. R. Zentner, and Z. Ma, J. Cosmol. Astropart. Phys. 4 (2012) 034.
[11] K. Heitmann, D. Higdon, M. White, S. Habib, B. J. Williams, E. Lawrence, and C. Wagner, Astrophys. J. **705**, 156 (2009).
[12] E. Lawrence, K. Heitmann, M. White, D. Higdon, C. Wagner, S. Habib, and B. Williams, Astrophys. J. **713**, 1322 (2010).
[13] K. Heitmann, M. White, C. Wagner, S. Habib, and D. Higdon, Astrophys. J. **715**, 104 (2010).
[14] T. Eifler, Mon. Not. R. Astron. Soc. **418**, 536 (2011).
[15] H. Zhan and L. Knox, Astrophys. J. Lett. **616**, L75 (2004).
[16] M. White, Astropart. Phys. **22**, 211 (2004).
[17] Y. P. Jing, P. Zhang, W. P. Lin, L. Gao, and V. Springel, Astrophys. J. Lett. **640**, L119 (2006).
[18] D. H. Rudd, A. R. Zentner, and A. V. Kravtsov, Astrophys. J. **672**, 19 (2008).
[19] T. Guillet, R. Teyssier, and S. Colombi, Mon. Not. R. Astron. Soc. **405**, 525 (2010).

[20] E. Semboloni, H. Hoekstra, J. Schaye, M. P. van Daalen, and I. G. McCarthy, Mon. Not. R. Astron. Soc. **417**, 2020 (2011).

[21] A. R. Zentner, D. H. Rudd, and W. Hu, Phys. Rev. D **77**, 043507 (2008).

[22] A. P. Hearin and A. R. Zentner, J. Cosmol. Astropart. Phys. 4 (2009) 32.

[23] D. Huterer and M. White, Phys. Rev. D **72**, 043002 (2005).

[24] J. C. Muñoz-Cuartas, A. V. Macciò, S. Gottlöber, and A. A. Dutton, Mon. Not. R. Astron. Soc. **411**, 584 (2011).

[25] F. Prada, A. A. Klypin, A. J. Cuesta, J. E. Betancort-Rijo, and J. Primack, Mon. Not. R. Astron. Soc. **423**, 3018 (2012).

[26] J. Schaye, C. Dalla Vecchia, C. Booth, R. P. Wiersma, T. Theuns, M. R. Haas, S. Bertone, A. R. Duffy, I. G. McCarthy, and F. van de Voort, Mon. Not. R. Astron. Soc. **402**, 1536 (2010).

[27] M. P. van Daalen, J. Schaye, C. Booth, and C. D. Vecchia, Mon. Not. R. Astron. Soc. **415**, 3649 (2011).

[28] A. Albrecht, G. Bernstein, R. Cahn, W. L. Freedman, J. Hewitt, W. Hu, J. Huth, M. Kamionkowski, E. W. Kolb, L. Knox *et al.*, arXiv:0609591.

[29] E. Semboloni, L. van Waerbeke, C. Heymans, T. Hamana, S. Colombi, M. White, and Y. Mellier, Mon. Not. R. Astron. Soc. **375**, L6 (2007).

[30] Z. Ma, W. Hu, and D. Huterer, Astrophys. J. **636**, 21 (2006).

[31] P. A. Abell, J. Allison, S. F. Anderson, J. R. Andrew, J. R. P. Angel, L. Armus, D. Arnett, S. J. Asztalos, T. S. Axelrod *et al.* (LSST Science Collaborations), arXiv:0912.0201.

[32] R. Laureijs, J. Amiaux, S. Arduini, J. Augueres, J. Brinchmann, R. Cole, M. Cropper, C. Dabin, L. Duvet, A. Ealet *et al.*, arXiv:1110.3193.

[33] J. A. Newman, M. C. Cooper, M. Davis, S. M. Faber, A. L. Coil, P. Guhathakurta, D. C. Koo, A. C. Phillips, C. Conroy, A. A. Dutton *et al.*, arXiv:1203.3192.

[34] M. Chevallier and D. Polarski, Int. J. Mod. Phys. D **10**, 213 (2001).

[35] W. Hu, D. Huterer, and K. M. Smith, Astrophys. J. Lett. **650**, L13 (2006).

[36] W. Hu and M. J. White, Astrophys. J. **554**, 67 (2001).

[37] M. White and W. Hu, Astrophys. J. **537**, 1 (2000).

[38] A. Cooray and W. Hu, Astrophys. J. **554**, 56 (2001).

[39] C. Vale and M. White, Astrophys. J. **592**, 699 (2003).

[40] S. Dodelson, C. Shapiro, and M. White, Phys. Rev. D **73**, 023009 (2006).

[41] L. Knox, R. Scoccimarro, and S. Dodelson, Phys. Rev. Lett. **81**, 2004 (1998).

[42] C. M. Booth and J. Schaye, Mon. Not. R. Astron. Soc. **398**, 53 (2009).

[43] R. P. C. Wiersma, J. Schaye, T. Theuns, C. D. Vecchia, and L. Tornatore, Mon. Not. R. Astron. Soc. **399**, 574 (2009).

[44] R. P. C. Wiersma, J. Schaye, and B. D. Smith, Mon. Not. R. Astron. Soc. **393**, 99 (2009).

[45] C. Dalla Vecchia and J. Schaye, Mon. Not. R. Astron. Soc. **387**, 1431 (2008).

[46] J. Schaye and C. Dalla Vecchia, Mon. Not. R. Astron. Soc. **383**, 1210 (2008).

[47] I. G. McCarthy, J. Schaye, T. J. Ponman, R. G. Bower, C. M. Booth, C. Dalla Vecchia, R. A. Crain, V. Springel, T. Theuns, and R. P. C. Wiersma, Mon. Not. R. Astron. Soc. **406**, 822 (2010).

[48] I. G. McCarthy, J. Schaye, R. G. Bower, T. J. Ponman, C. M. Booth, C. Dalla Vecchia, and V. Springel, Mon. Not. R. Astron. Soc. **412**, 1965 (2011).

[49] R. Stanek, D. Rudd, and A. E. Evrard, Mon. Not. R. Astron. Soc. **394**, L11 (2009).

[50] J. F. Navarro, C. S. Frenk, and S. D. M. White, Astrophys. J. **490**, 493 (1997).

[51] A. F. Neto, L. Gao, P. Bett, S. Cole, J. F. Navarro, C. S. Frenk, S. D. M. White, V. Springel, and A. Jenkins, Mon. Not. R. Astron. Soc. **381**, 1450 (2007).

[52] A. V. Macciò, A. A. Dutton, F. C. van den Bosch, B. Moore, D. Potter, and J. Stadel, Mon. Not. R. Astron. Soc. **378**, 55 (2007).

[53] A. V. Macciò, A. A. Dutton, and F. C. van den Bosch, Mon. Not. R. Astron. Soc. **391**, 1940 (2008).

[54] A. R. Duffy, J. Schaye, S. T. Kay, and C. Dalla Vecchia, Mon. Not. R. Astron. Soc. **390**, L64 (2008).

[55] A. R. Duffy, J. Schaye, S. T. Kay, C. Dalla Vecchia, R. A. Battye, and C. M. Booth, Mon. Not. R. Astron. Soc. **405**, 2161 (2010).

[56] G. M. Bernstein, Astrophys. J. **695**, 652 (2009).

[57] T. D. Kitching and A. N. Taylor, Mon. Not. R. Astron. Soc. **416**, 1717 (2011).

[58] B. Jain and A. Taylor, Phys. Rev. Lett. **91**, 141302 (2003).

[59] J. Zhang, L. Hui, and A. Stebbins, Astrophys. J. **635**, 806 (2005).